Dielectric anomaly at the orbital order–disorder transition in $LaMnO_{3+\delta}$

2006 J. Phys.: Condens. Matter 18 6869

(http://iopscience.iop.org/0953-8984/18/29/024)

INSTITUTE OF PHYSICS PUBLISHING JOURNAL OF PHYSICS: CONDENSED MATTER

J. Phys.: Condens. Matter **18** (2006) 6869–6881 doi:10.1088/0953-8984/18/29/024

Dielectric anomaly at the orbital order–disorder transition in $LaMnO_{3+\delta}$

Parthasarathi Mondal, Dipten Bhattacharya and Pranab Choudhury

Electroceramics Division, Central Glass and Ceramic Research Institute, Calcutta 700 032, India

E-mail: dipten@cgcri.res.in

Received 7 April 2006
Published 6 July 2006
Online at stacks.iop.org/JPhysCM/18/6869

Abstract

We report a novel dielectric anomaly around the Jahn–Teller orbital order–disorder transition temperature T_{JT} in $LaMnO_{3+\delta}$. The transition has been characterized by resistivity (ρ) versus temperature (T), calorimetry, and temperature dependent x-ray diffraction studies. Measurements of complex dielectric permittivity ε^* ($= \varepsilon' - i\varepsilon''$) over a low-frequency range (1 Hz–10 MHz) across T_{JT} reveal a distinct anomaly. This observation, and the reported relatively high static dielectric constant at $T = 0$ ($\varepsilon_0 \sim 18$–20), possibly indicate that the orbital order gives rise to intrinsic polarization that undergoes transition at T_{JT}. The frequency dispersion of the dielectric response at any given temperature, however, reveals that the dielectric response consists of Maxwell–Wagner component, due to interfaces, within such a low frequency range. The T_{JT} and the nature of the anomaly in $\varepsilon'(\omega, T)$, $\varepsilon''(\omega, T)$ at T_{JT}, of course, vary—from a sharp upward feature to a smeared plateau and then a downward trend—depending on the Mn^{4+} concentration of the sample. The observation of an intrinsic dielectric response due to long-range orbital order in $LaMnO_3$—where no ferroelectric order is possible due to the absence of off-centre distortion in MnO_6 octahedra—may throw a new light onto these classes of materials vis-à-vis multiferroic materials.

1. Introduction

Recent progress in research on different orbital phases and their correlation with charge and spin phases sheds light on the close interplay between charge, spin, orbital and lattice degrees of freedom in rare-earth perovskite manganites [1]. It has been realized, though not quantitatively established, that the orbital order governs the nature of the charge and spin order. The onset of orbital order at a higher temperature appears to be a necessary prerequisite for the onset of charge or spin order at a lower temperature in many cases. The temperature gap varies and even collapses for some strongly correlated systems like $LaTiO_3$ [2]. Hence, proper understanding

and characterization of the orbital phases and phase transitions assumes significance. It has already been pointed out and experimentally observed that the orbital order could either be long range or short range [3]. In other words, orbital domain size may vary depending on the structural distortion. The estimation of spatio-temporal fluctuation of the orbital domains as a function of lattice distortion and temperature seems to be quite important in characterizing the orbital phases. Related to the orbital domain size and temporal fluctuation is the nature of the order–disorder transition at a characteristic transition point. We have shown recently that with the increase in geometric lattice distortion or tilt order due to decrease in average A-site radius $\langle r_A \rangle$, the latent heat associated with the transition decreases and finally reaches zero [4]. We have also noticed that irrespective of the A-site rare-earth ion, the latent heat becomes zero at a critical $\langle r_A \rangle_c \approx 1.180$ Å [5]. The pattern of the drop, however, varies with ion type, which interestingly can be made to collapse onto a universal pattern for a suitable choice of scaling parameter.

The broadband dielectric spectroscopy helps in characterizing the phase transitions in doped Mott insulator systems like cuprates (the parent compounds of high-T_c superconductors) [6], manganites (both hole and electron doped) [7–10], other non-oxide spinel systems [11] etc, which are have relatively low resistivity and are not traditionally used as dielectrics. In systems where one might observe glass transition, dielectric spectroscopy assumes significance in evaluating the relaxation timescale across the phase transition point and correlating the relaxation dynamics with microscopic features. Since in pure manganites the latent heat drops with the drop in $\langle r_A \rangle$ and becomes zero [4, 5], it seems that the orbital domain size also decreases with $\langle r_A \rangle$ and eventually an *orbital glass* phase evolves beyond $\langle r_A \rangle_c$. One can possibly distinguish between glassy dynamics and dynamics of the systems with long-range order using dielectric spectroscopy [11]. The static long-range orbital order phase should relax slowly and, therefore, can be probed by a low-frequency signal, while a disordered phase with short-range order is expected to relax faster and hence should be probed by a higher-frequency signal. The relaxation timescale may vary depending on the orbital domain size. The extension of the energy scale of the probe from low to the optical range helps in covering the entire spatio-temporal range of the orbital order: from long-range slower modes of the entire orbital order network to faster local phonon and local orbiton modes around the Jahn–Teller active Mn^{3+} ions in the optical range. The IR- and Raman-active phonon and orbiton modes have been studied in $LaMnO_3$ as a function of temperature by other authors [12–14]. However, to the best of our knowledge, no report so far exist in the published literature on the low-frequency dielectric response of $LaMnO_3$ near the orbital order–disorder transition. Therefore, we attempt to study the phase transition features using low-frequency dielectric spectroscopy in pure $LaMnO_{3+\delta}$ with long-range orbital order as a first step towards unveiling the phase transition dynamics across the entire range of $\langle r_A \rangle$.

In this paper, we report our results on the dielectric anomaly at the orbital order–disorder transition temperature (T_{JT}) in pure $LaMnO_{3+\delta}$ having varying Mn^{4+} concentration. The T_{JT} as well as the nature of the anomaly varies with the Mn^{4+} concentration. We probe primarily the dielectric response arising out of space charge and intrinsic polarization within the frequency window used in this work. In polycrystalline samples, interface polarization results from inhomogeneous regions due to insulating grain boundaries and conducting grains. We notice that at a given temperature the overall dielectric response, across the frequency range, is dominated, essentially, by Maxwell–Wagner relaxation dynamics arising as a result of such interfaces even though the intrinsic polarization, due possibly to orbital order, also has a significant influence. The sharp feature in the dielectric response at T_{JT} becomes smeared with the increase in Mn^{4+} concentration.

2. Experiments and results

The experiments have been carried out on high-quality bulk polycrystalline $LaMnO_{3+\delta}$ samples. Details of the sample preparation were given in our earlier papers [4, 15]. The Mn^{4+} concentration has been varied by treating the samples under different atmospheres: air, air + N_2 or air + Ar, and pure Ar. The orbital order–disorder transition was characterized by four-probe dc resistivity versus temperature measurements, calorimetry using DTA-50 (Shimadzu) and Diamond DSC (Perkin–Elmer), and temperature dependent x-ray diffraction (XRD) study. The Mn^{4+} concentration was estimated from chemical analysis (redox titration). The XRD patterns of the samples at different temperatures were recorded on a Philips X-Pert Pro diffractometer, with an Anton Parr high-temperature attachment. Rectangular bar-shaped samples of typical dimensions 15 mm × 5 mm × 1.5 mm have been used for resistivity measurements. The current leads and voltage probes were made of high-quality platinum paste and platinum wires. The contacts were cured overnight at around 1100 °C under an appropriate atmosphere. The dielectric measurements were carried out using a Solartron (model 1260) frequency response analyser (FRA) coupled with a dielectric interface (model 1296A) across a temperature regime of 300–950 K with the help of Impedance Spectroscopy software. The applied field amplitude was varied over 0.1–1 V. However, no dependence of the dielectric response pattern could be noticed as a result of such variation. We have also studied the dielectric response at ∼77 K in order to compare our data with the data for similar systems measured by others [7] at ∼77 K. The measurement across T_N (∼140 K) in pure $LaMnO_3$ reveals a significant dielectric anomaly near T_N that possibly reflects the spin–orbital coupling [16]. The electrodes have been made of high-quality platinum, gold and vapour deposited silver. Data obtained for different electrodes were compared in order to extract the intrinsic features of the samples. The contribution of the instrument, cable and lead to the dielectric data have been carefully subtracted. Since the samples are basically of low resistivity, we employed the constant current mode for measurement of the dielectric response [7]. However, we have noticed that interface polarization, and hence the Maxwell–Wagner contribution, plays a major role in determining the dielectric permittivity and its frequency dependence in all cases. The intrinsic capacitive response is small at room temperature. In spite of such a poor response, we noticed a distinct anomaly at T_{JT} in both the real and the imaginary part of the dielectric permittivity. Therefore, it appears that dielectric spectroscopy can be successfully used to study the orbital order–disorder transition in different rare-earth perovskite manganites.

The Mn^{4+} concentrations for the four samples—sample 1 (T_{JT} ∼ 730 K), sample 2 (T_{JT} ∼ 718 K), sample 3 (T_{JT} ∼ 703 K) and sample 4 (T_{JT} ∼ 653 K)—are 2% ± 0.3%, 5%±0.6%, 9%±0.7% and 15%±1.2%, respectively. In figure 1, we show the x-ray diffraction (XRD) patterns of a representative sample (sample 1) collected at different temperatures—at room temperature (i.e. below T_{JT}) and above T_{JT}—and their Rietveld refinement by Fullprof (ver 2.3, 1999). The refinement parameters, including the results like atomic positions etc, are mentioned in table 1. In figure 2, we show the variation of lattice parameters and lattice volume with Mn^{4+} concentration at room temperature [17]. And the variation of the relevant parameters with temperature for samples 1 and 4 is shown in figure 3. Across the transition point it is found that the low-temperature orthorhombic O′ phase ($c/\sqrt{2} < a < b$) becomes an orthorhombic O phase ($c/\sqrt{2} > a \approx b$) at higher temperature. The temperature dependent x-ray diffraction study yields the volume collapse ($\Delta V/V$) at T_{JT} to be ∼0.3% for sample 1 and ∼0.016% for sample 4 [18]. The orthorhombic distortion is found to drop from ∼2.1% to ∼0.045% over a temperature regime of 300–773 K for sample 1 and from ∼1.05% to ∼0.13% over a temperature regime of 300–723 K for sample 4. In figure 4, we show the resistivity (ρ) versus temperature (T) patterns for all the samples. The temperature range, marked by

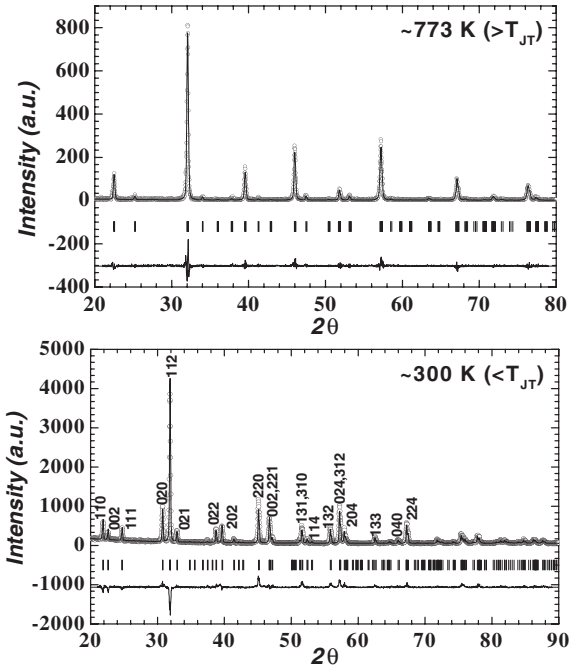

Figure 1. X-ray diffraction patterns—refined by Fullprof (ver 2.3, 1999)—for sample 1 at below and above T_{JT} (∼300 and 773 K). The open circles denote the experimental data points.

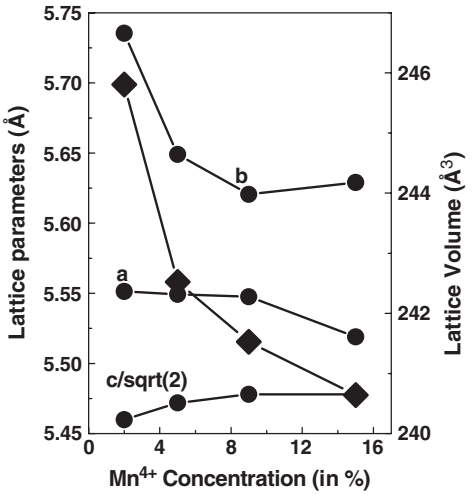

Figure 2. Variation of lattice parameters and lattice volume (♦) at room temperature as a function of Mn^{4+} concentration in $LaMnO_{3+\delta}$.

two transition points T^* and T_{JT}, can be considered as the orbital order–disorder transition zone. T^* and T_{JT} define the onset [19] and completion of the transition, respectively. They are plotted as a function of Mn^{4+} concentration in the top inset of figure 4. As expected, they drop systematically with the increase in Mn^{4+} concentration. The bottom inset shows the $\ln(\rho/T)$ versus $1/T$ plots. A linear $\ln(\rho/T)$ versus $1/T$ pattern highlights the validity

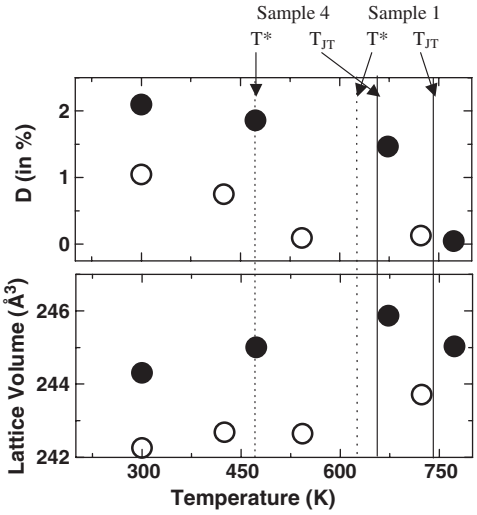

Figure 3. Variation of lattice volume and orthorhombic distortion D as a function of temperature for samples 1 (●) and 4 (○). The orthorhombic distortion D is given by $D = [|(a - a_1)| + |(b - a_1)| + |(c/\sqrt{2} - a_1)|]/3a$, where $a_1 = (abc/\sqrt{2})^{1/3}$. The transition temperatures T^* and T_{JT} are marked as identified from resistivity versus temperature data.

Table 1. Results of the Rietveld refinement of the x-ray diffraction patterns for samples 1 and 4 at a few selective temperatures below and above transition (T_{JT}). The atomic positions are: La (x, y, 0.25), Mn (0.5, 0, 0), O1 (x, y, 0.25), O2 (x, y, z). The space group is $Pbnm$.

		La		O1		O2					
	T (K)	x	y	x	y	x	y	z	R_p	R_{wp}	χ^2
Sample 1	300	0.99334	0.04599	0.05062	0.50187	0.72115	0.30422	0.02602	13.8	17.0	3.49
($T_{JT} \sim 730$ K)	673	0.9939	0.04072	0.0683	0.49388	0.71684	0.2986	0.0282	20.1	28.7	1.20
	773	0.99377	0.02631	0.06205	0.50085	0.78503	0.22204	−0.0181	19.4	28.6	1.15
Sample 4	300	0.99487	0.03569	0.04833	0.49967	0.74036	0.28979	0.03289	14.9	20.3	3.22
($T_{JT} \sim 653$ K)	543	0.99331	0.02405	0.03882	0.50070	0.73557	0.26752	0.01676	14.4	18.7	2.55
	723	0.98933	0.01344	0.0189	0.49735	0.75026	0.30001	−0.0002	17.8	23.6	3.96

of an adiabatic small polaron hopping transport mechanism—$\rho(T) = \rho_0 T \exp(E_a/k_B T)$—over a certain temperature range. Below T^* and above T_{JT}, the $\ln(\rho/T)$ versus $1/T$ patterns follow straight lines. As shown in the bottom inset of figure 4, T^* marks the onset of deviation of the $\ln(\rho/T)$ versus $1/T$ pattern from a straight line while T_{JT} is evaluated as the point above the transition at which the pattern starts following the straight line. The transition zone becomes broader with increase in Mn^{4+} concentration. T_{JT} evaluated from thermal studies (differential thermal analysis or differential scanning calorimetry) nearly coincides with the T_{JT} evaluated from resistivity plots. The uncertainty in T_{JT}, estimated from both resistivity and thermal studies, and in T^*, estimated from resistivity patterns, is mentioned in figure 4 (top inset) as error bars. The adiabatic small polaron hopping mechanism appears to be valid at below T^* and above T_{JT}, with different activation energies. The activation energies (E_a), below T^* and above T_{JT}, are estimated to be ∼2550 K, ∼4100 K; ∼2920 K, 3180 K; ∼2920 K, ∼3230 K; and ∼2690 K, ∼3170 K for the samples with $T_{JT} \sim 730$ K (sample 1), ∼718 K (sample 2), ∼703 K (sample 3), and ∼653 K (sample 4), respectively. In figure 5, we show

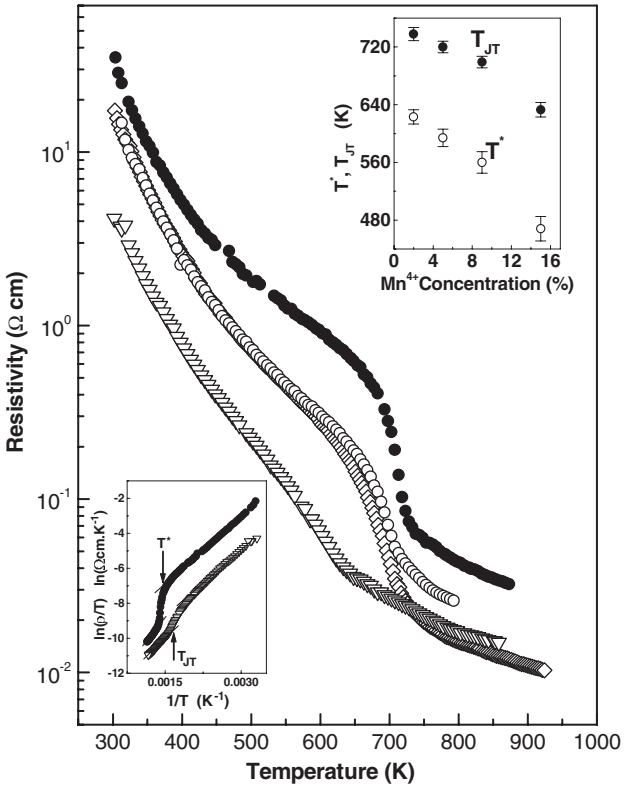

Figure 4. Resistivity versus temperature plots for sample 1 (●; $T_{JT} \sim 730$ K); sample 2 (○; $T_{JT} \sim 718$ K); sample 3 (◇, $T_{JT} \sim 700$ K); sample 4 (▽, $T_{JT} \sim 653$ K). The top inset shows the variation in T^*, T_{JT} with Mn^{4+} concentration and the bottom inset shows $\ln(\rho/T)$ versus $1/T$ plot for samples 1 and 4.

the DTA patterns depicting endothermic peaks at corresponding T_{JT}. While the thermograms corresponding to the samples 1, 2 and 3 are shown in the main frame, the thermogram for sample 4 is shown in the top inset since the peak near the transition is almost an order of magnitude smaller. The DTA thermograms have been measured with an α-alumina reference. A drift in the baseline is observed in some cases because of the difference in heat capacity. However, through proper baseline correction one can remove the drift. In fact, in order to clearly display the peak near T_{JT} for sample 4, we refined the thermogram corresponding to sample 4 (top inset) by baseline correction. The latent heat is calculated, for all the cases, from the area under the peak after correcting the baseline of the raw thermograms. In the bottom inset, we show the latent heat versus Mn^{4+} concentration. The latent heat drops with the increase in Mn^{4+} concentration. However, one interesting point worth noting is that even in a sample with large Mn^{4+} concentration (sample 4), the latent heat does not become zero. It has been pointed out previously [20] that the first-order transition gives way to a second-order transition for a very low Mn^{4+} concentration ($\sim$2.5%) in Ba-doped $LaMnO_3$. It seems that the Mn^{4+} concentration is not the only factor that governs the nature of the transition; Ba-doping and consequent disorder also plays an important role in determining the nature of the transition.

In figures 6(a)–(f), we show the real and imaginary parts of the permittivity $\varepsilon'(\omega, T)$, $\varepsilon''(\omega, T)$ as a function of temperature for all the samples. In both $\varepsilon'(\omega, T)$ and $\varepsilon''(\omega, T)$ a

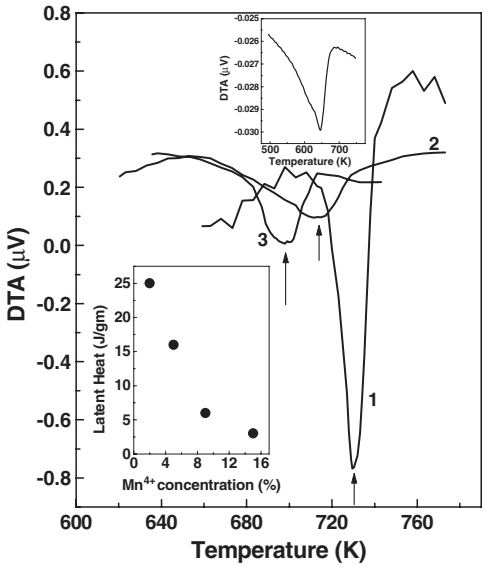

Figure 5. DTA thermograms for samples 1, 2 and 3. The top inset shows the thermogram for samples 4 and the bottom inset shows the variation in latent heat with Mn^{4+} concentration.

distinct anomaly could be observed at T_{JT} in the case of all four samples. This observation and the reported [8] reasonably large static dielectric constant of $LaMnO_3$ at $T = 0$ can be taken as signatures of formation of orbital order induced intrinsic polarization. In this paper, we present only this relative variation of the nature of the anomaly at T_{JT} by comparing the data observed in different samples.

3. Discussion

The pure $LaMnO_3$ contains a C-type orbital-ordered phase while with the increase in Mn^{4+} concentration, the volume fraction of the orbital-disordered phase increases. The transition at T_{JT}, therefore, evolves as a function of volume fraction of the disordered phase. The transition zone bound by the temperatures T^* and T_{JT} also extends with the increase in Mn^{4+} concentration (top inset of figure 4). The activation energy E_a—obtained from the dc resistivity versus temperature data by using a small polaron hopping transport model—at below T^* (E_{aT^*}) and above T_{JT} ($E_{aT_{JT}}$) appears to exhibit a mutually opposite trend with variation in Mn^{4+} concentration: while E_{aT^*} increases with the increase in Mn^{4+} concentration, $E_{aT_{JT}}$ decreases. This shows that even though the charge carrier concentration increases and, therefore, the overall electrical resistivity decreases, the mobility of the charge carriers, in fact, decreases below T^* with the increase in Mn^{4+} concentration. On the other hand, the drop in $E_{aT_{JT}}$ with increase in Mn^{4+} concentration signifies higher mobility and, therefore, the relevance of vibronic charge carriers (mobile vibrons formed by charge carriers coupled with locally cooperative lattice vibration) at above T_{JT} [21]. The calorimetric data show how the latent heat associated with the order–disorder transition drops with the increase in Mn^{4+} concentration (figure 5). The observation of first-order transition with finite latent heat for all the samples is corroborated by the temperature dependent XRD study. In the case of sample 1, the finite lattice volume contraction ($\sim$0.3%) is observed between the points around T_{JT} (figure 3). The contraction signifies a first-order transition. In the case of sample 4, of course, a much smaller

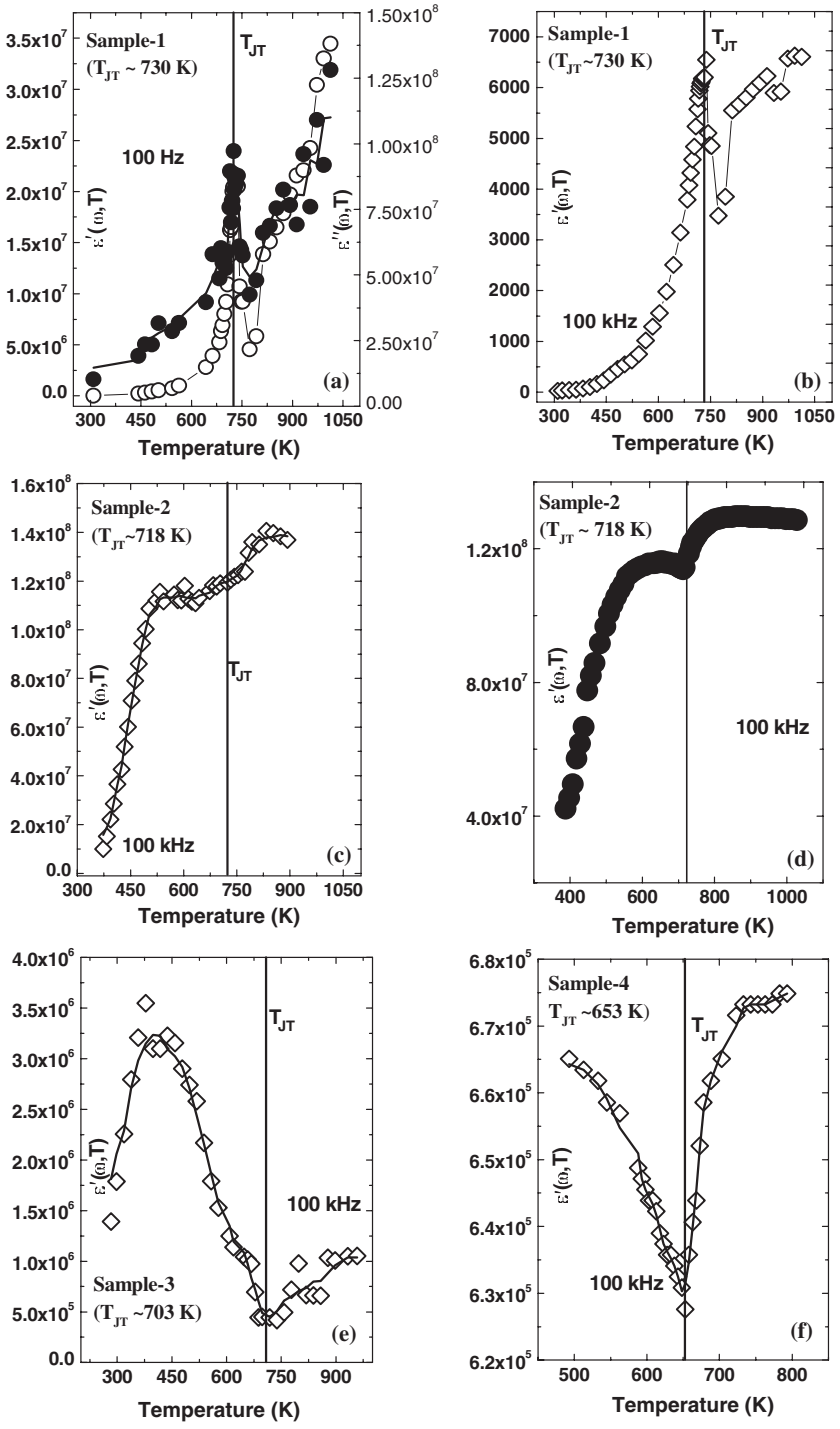

Figure 6. The real part of the dielectric permittivity for samples 1–4. In frame (a) the imaginary part of the dielectric permittivity, for sample 1, is also shown (solid symbols) as an example. In frame (d) the data from Au-coated sample-2 are shown. Data corresponding to other frames have been obtained from samples with Pt electrodes.

contraction (∼0.016%) is observed between the points near T^*. In this case, the orthorhombic distortion also decreases between room temperature and 543 K. Beyond T_{JT} (∼653 K) the lattice volume depicts an increase whereas the orthorhombic distortion remains small (figure 3).

We now concentrate on the dielectric response of the samples. The following facts are evident in the data presented in figure 6. (a) There are clear anomalies near the corresponding T_{JT}s for all the samples. (b) The nature of the anomaly at T_{JT} varies with the increase in Mn^{4+} concentration following a certain trend—from a sharp upward feature to a smeared plateau and then a downward feature to finally, a rather broader downward peak. (c) There is a large frequency dispersion of the real and imaginary permittivity, at any given temperature, which reveals the dominance of Maxwell–Wagner relaxation behaviour within the frequency domain used here [22]. This is due to interfaces formed by conducting grains and insulating grain boundaries. No characteristic Debye relaxation peak could be observed in $\varepsilon''(\omega)$. (d) The pattern of temperature dependence of the real and imaginary permittivity varies from sample to sample as the contribution from the intrinsic polarization varies with temperature. (e) The temperature dependence of permittivity as well as the nature of the dielectric anomaly at respective T_{JT} does not vary much with variation in electrode—Pt, Au, Ag. *These are the central results of this paper*. In figure 6(d), we show $\varepsilon'(\omega, T)$ for sample 2 with an Au electrode. The general features like rise in $\varepsilon'(\omega, T)$ with temperature and a bend and, finally, a rise beyond T_{JT} are present in both sets of data—recorded for sample 2 with Pt and Au electrodes. The slight difference noticed in the feature near the anomaly could be due to difference in adhesion of the electrodes. The Au electrode appears to offer better adhesion. In the case of sample 4, a prominent anomaly near T_{JT} is observed at higher frequency ($\geqslant$100 kHz). The lower-frequency data (not shown) reveal a kink-like anomaly and not a prominent one. This could be because at higher Mn^{4+} concentration, the volume fraction of the orbital ordered phase decreases, and hence a higher-frequency ac probe is required in order to track the orbital order–disorder transition. In fact, the local dynamic Jahn–Teller distortion can only be studied by an optical probe [23].

We first address the issue of the dielectric contribution from contacts and other interfaces like grain boundaries and intrinsic interfaces, if any. The $\varepsilon'(\omega)$, $\varepsilon''(\omega)$ show a large frequency dispersion within the frequency window used in this work. Both $\varepsilon'(\omega)$, $\varepsilon''(\omega)$ tend to higher values as $\omega \rightarrow 0$ without showing any clear relaxation feature. This could be due to a combination of the following factors: (i) large frequency dispersion of the interface polarization, (ii) non-trivial frequency dependence of intrinsic resistance (R) and capacitance (C) elements due to essentially non-Debye type dielectric relaxation, (iii) relaxor-type behaviour of the intrinsic polarization. The contribution of the interface polarization normally dominates the overall response in such low-resistive polycrystalline samples. However, the complex plane analysis of the impedance spectra does not help in separating the relaxation spectrum of interface and intrinsic polarization within the temperature range explored in this work. Consequently, we could not estimate the *intrinsic* dielectric permittivity and the relaxation timescale (τ) across the temperature range of this study. Even comparison of different formalisms, like impedance (Z', Z''), permittivity (ε', ε'') and modulus (M', M'') does not help in determining these parameters. Extension of the frequency range beyond 1 MHz may help in observing the full relaxation spectrum corresponding to the intrinsic polarization in the frequency domain. It is to be noted that the full relaxation spectrum corresponding to intrinsic polarization could be observed only at lower temperatures (77–250 K) within the frequency window used (10 Hz–1 MHz) [16]. Near 250 K, the relaxation feature shifts to an even higher frequency. It is also noteworthy, in this context, that because of such dominance of the Maxwell–Wagner effect, the real and imaginary permittivities assume a very high value ($>10^7$). Such colossal values could be observed in other such strongly correlated systems

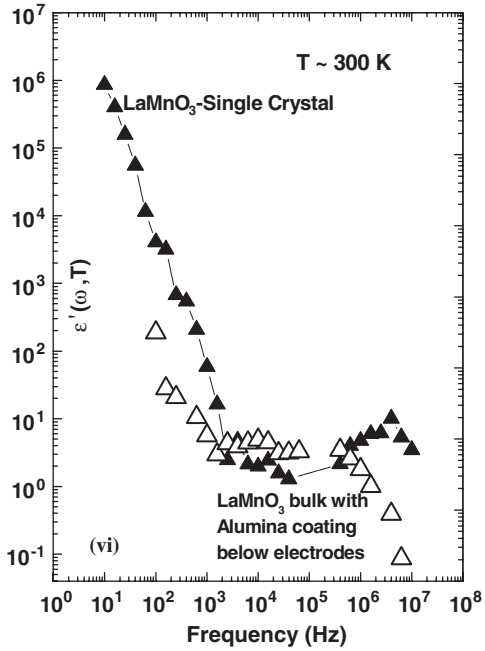

Figure 7. The typical frequency dispersion pattern of the real part of the dielectric permittivity observed in single crystal $LaMnO_3$ and a bulk polycrystalline sample coated with alumina. In both the cases a Pt electrode has been used.

having mobile charge carriers [6–11]. It seems that in all the cases such large values result from interfaces, and therefore are not intrinsic. In fact, further work seems necessary in order to extract the intrinsic dielectric permittivity as well as its relaxation in these systems. Here, of course, we are concerned more with a relative comparison of the data as a function of Mn^{4+} concentration, in a series of pure $LaMnO_3$ systems, than with the absolute values of the intrinsic permittivity. However, in order to get a fairly reliable idea about the relative contribution of contacts and other interfaces to the overall dielectric response and its frequency dispersion, we carried out measurements on a single crystal of $LaMnO_3$, a bulk polycrystalline sample coated with alumina, and bulk samples coated with different electrodes like Au, Ag and Pt without an alumina layer. In the cases of the single crystal and alumina-coated samples, Pt electrodes were used. The single crystal is expected to be free of grain boundaries while the alumina coating on bulk sample is expected to suppress the spurious capacitance due to contacts [6]. The suppression of spurious capacitance at the contacts, of course, cannot be total, as depending on the thickness ratio between the bulk and coating one can observe finite frequency dispersion of dielectric permittivity even in this case. The dielectric spectra at room temperature for these cases are shown in figure 7 as an example. It is quite clear from the spectra in figure 7 that both the single crystal and the alumina-coated bulk sample exhibit lesser frequency dispersion compared to bulk uncoated samples. Comparison of these data with the data obtained for bulk polycrystalline samples with different electrodes (Au, Ag, Pt) and without alumina coating provides a rough estimation of the relative contribution of the contacts and other interfaces. It appears that nearly two orders of magnitude dispersion in dielectric permittivity, over a frequency range of four orders, results from the intrinsic polarization contribution. Therefore, we conclude that as well as Maxwell–Wagner relaxation due to interfaces there is a *sizable*

component of intrinsic polarization dispersion across the entire frequency window used here. This dispersion could result from either non-trivial frequency dependence of R and C or relaxor-like behaviour or a combination of both. At any given frequency within this range, the overall dielectric permittivity is given by the summation of the intrinsic and interfacial permittivity normalized by the ratio of the logarithm of volumes (Lichteneckar's rule).

We now turn our attention to the nature of the dielectric anomaly at T_{JT} and its variation with the increase in Mn^{4+} concentration. The increase in Mn^{4+} concentration gives rise to a decrease in volume fraction of the orbital ordered phase that, in turn, results in such an evolution in the nature of the anomaly. The shift from an upward feature to a downward one is intriguing. An upward anomaly is observed in multiferroic $TbMnO_3$, $DyMnO_3$ [24] where as in the case of $BiFeO_3$, one observes a downward anomaly [25] and its smearing with the increase in non-stoichiometric oxygen [26]. In all these cases, of course, the dielectric anomalies are observed near the Néel point T_N and signify magneto-electric coupling. In the present case, the dielectric anomaly near T_{JT} signifies a transition in orbital-order-driven electrical polarization. A quantitative estimation of the anomaly as a function of Mn^{4+} concentration is possible only if we could correlate the orbital domain size with the local electrical polarization length in samples having different Mn^{4+} concentration. The orbital domain size is expected to become smaller with the increase in Mn^{4+} concentration that, in turn, is expected to give rise to a systematic variation in electrical polarization length scale. This detailed study is beyond the scope of the present work.

Finally, we point out that for non-polar systems, one observes the static dielectric constant (ε_0) at $T = 0$ to be within 1–5. It has already been reported [8], however, that for $LaMnO_3$, ε_0 is within 18–20, which is reasonably high. This gives an indication that intrinsic polarization probably develops *locally*. Since $LaMnO_3$ is *globally* centrosymmetric, it cannot exhibit a very high dielectric constant in the global scale. However, because of the cooperative Jahn–Teller effect together with tilt order due to the La-site radius, one can predict *local* breakdown of the centrosymmetry and the development of dipoles due to charge separation in the Mn–O plane. The correlation among local Mn–O bond distortion due to orbital order and charge displacement giving rise to local dipoles has been established in [16]. Another important point worthy of mention here is that both the temperature dependence of $\varepsilon'(\omega)$ and the anomalies at T_{JT} vary from sample to sample. This is unexpected in an essentially non-polar system. The volume fraction of the orbital ordered phase certainly has a role to play here. Piecing together all these features, it is possible to conclude that long-range orbital order gives rise to non-trivial intrinsic polarization even in a globally centrosymmetric compound like $LaMnO_3$. Yang *et al* [27] have pointed out the relevance of orbital-order-driven polarization in $BiMnO_3$ very recently. Another example is the electronic mechanism (charge order)-driven polarization that is found to have given rise to long-range ferroelectric order in $LuFe_2O_4$ [28]. Our observation of the dielectric anomaly within the low-frequency range (100 Hz–1 MHz) together with large frequency dispersion and frequency dependence of the nature of the anomaly points out that intrinsic polarization develops, at least, *locally* because of orbital order. Additional structural distortion due to either stereo-chemical activity of the Bi $6s^2$ lone pair in $BiMnO_3$ and $BiFeO_3$ or the MnO_5 bi-pyramid in $RMnO_3$ (R = Dy, Tb, Y, Yb, Lu etc) or the electron correlation effect in charge-ordered $LuFe_2O_4$ gives rise to global ferroelectricity. The long-range polarization length scale may vary depending on the presence or absence of the additional mechanism along with the long-range orbital order. Alongside, the extent of dispersion in intrinsic dielectric permittivity also varies depending on the polarization length scale. It will be interesting to study how the polarization length scale grows as a result of systematic increase in structural distortion in the presence of long-range orbital order. This will be attempted in a future study.

4. Summary

In summary, we have indicated that there is a possibility of observing orbital-order-driven intrinsic electrical polarization in pure $LaMnO_{3+\delta}$. As a result, one observes a distinct dielectric anomaly at the transition temperature T_{JT}. The Maxwell–Wagner effect arising out of interfaces and/or mobile charge carriers, of course, dominates the overall dielectric response in the temperature and frequency range covered in this work. However, the temperature dependence of the real and imaginary permittivity as well as the variation in the nature of the anomaly at T_{JT} from sample to sample reveals the influence of intrinsic orientation polarization due to orbital order. The transition temperature itself and the latent heat associated with the transition decrease with the Mn^{4+} concentration, yet interestingly they do not become zero, at least over the range of Mn^{4+} concentrations studied here. This shows that one can play with the relative volume fraction of orbital ordered and disordered phases and learn about the phase transition from dielectric relaxation across the T_{JT} in all such insulating manganites exhibiting an orbital order–disorder transition. Further work at an even higher frequency range (>1 MHz) seems to be necessary in order to estimate the intrinsic dielectric constant as well as its relaxation dynamics. Such results may spur more work aimed towards discovering the driving mechanism behind intrinsic polarization observed in these centrosymmetric compounds.

Acknowledgments

We acknowledge the help of P S Devi of CGCRI in estimation of the Mn^{4+} concentration by chemical analysis and A K Tyagi of BARC, Mumbai, India for carrying out the x-ray diffraction studies at different temperatures. We also thank P Mandal of SINP, Calcutta, India for providing the single crystal of $LaMnO_3$.

References

[1] Tokura Y and Nagaosa N 2000 *Science* **280** 462
van den Brink J, Khaliullin G and Khomskii D I 2002 *Colossal Magnoresistive Manganites* ed T Chatterji (Dordrecht: Kluwer)
Khomskii D I 2005 *Phys. Scr.* **72** CC8–14
[2] Hemberger J, von Nidda H-A K, Fritsch V, Deisenhofer J, Lobina S, Rudolf T, Lunkenheimer P, Lichtenberg F, Loidl A, Bruns D and Büchner B 2003 *Phys. Rev. Lett.* **91** 066403
[3] Nelson C S, Hill J P, Gibbs D, Yakhou F, Livet F, Tomioka Y, Kimura T and Tokura Y 2002 *Phys. Rev.* B **66** 134412
[4] Bhattacharya D, Devi P S and Maiti H S 2004 *Phys. Rev.* B **70** 184415
[5] Mondal P and Bhattacharya D 2006 *Phys. Rev.* B submitted
[6] Park T, Nussinov Z, Hazzard K R A, Sidorov V A, Balatsky A V, Sarrao J L, Cheong S-W, Hundley M F, Lee J-S, Jia Q X and Thompson J D 2005 *Phys. Rev. Lett.* **94** 017002
[7] Mercone S, Wahl A, Pautrat A, Pollet M and Simon C 2004 *Phys. Rev.* B **69** 174433
[8] Cohn J L, Peterca M and Neumeier J J 2004 *Phys. Rev.* B **70** 214433
[9] Lunkenheimer P, Rudolf T, Hemberger J, Pimenov A, Tachos S, Lichtenberg F and Loidl A 2003 *Phys. Rev.* B **68** 245108
See also Cohn J L, Peterca M and Neumeier J J 2005 *J. Appl. Phys.* **97** 034102
[10] Fichtl R, Tsurkan V, Lunkenheimer P, Hemberger J, Fritsch V, von Nidda H-A K, Scheidt E-W and Loidl A 2005 *Phys. Rev. Lett.* **94** 027601
[11] Freitas R S, Mitchell J F and Schiffer P 2005 *Phys. Rev.* B **72** 144429
[12] Saitoh E, Okamoto S, Takahashi K T, Tobe K, Yamamoto K, Kimura T, Ishihara S, Maekawa S and Tokura Y 2001 *Nature* **410** 180
[13] Grüninger M, Rückamp R, Windt R, Reutler P, Zobel C, Lorenz T and Revcolevschi A 2002 *Nature* **418** 39
Saitoh E, Okamoto S, Tobe K, Yamamoto K, Kimura T, Ishihara S, Maekawa S and Tokura Y 2002 *Nature* **418** 40

[14] Krüger R, Schulz B, Naler S, Rauer R, Budelmann D, Bäckström J, Kim K H, Cheong S-W, Perebeinos V and Rübhausen M 2004 *Phys. Rev. Lett.* **92** 097203
[15] Bhattacharya D and Maiti H S 2002 *Phys. Rev.* B **66** 132413
Bhattacharya D, Das P, Pandey A, Raychaudhuri A K, Chakraborty A and Ojha V N 2001 *J. Phys.: Condens. Matter* **13** L431
[16] Mondal P, Bhattacharya D, Choudhury P and Mandal P 2006 *Phys. Rev.* B submitted
[17] The $LaMnO_{3+\delta}$ lattice volume decreases with increase in Mn^{4+} concentration. See, Van Roosmalen J A M and Cordfunke E H P 1994 *J. Solid State Chem.* **110** 106
[18] The lattice volume collapse for single crystals could be as high as ∼1%. See, Chatterji T, Fauth F, Ouladdiaf B, Mandal P and Ghosh B 2003 *Phys. Rev.* B **68** 052406
[19] Zhou J–S and Goodenough J B 2003 *Phys. Rev.* B **68** 144406
[20] Chatterji T, Ouladdiaf B, Mandal P and Ghosh B 2004 *Solid State Commun.* **131** 75
[21] Zhou J-S and Goodenough J B 1999 *Phys. Rev.* B **60** R15002
[22] See, for example, Jonscher A K 1977 *Nature* **267** 673
See also O'Neill D, Bowman R M and Gregg J M 2000 *Appl. Phys. Lett.* **77** 1520
[23] Iliev M N, Abrashev M V, Lee H-G, Popov V N, Sun Y Y, Thomsen C, Meng R L and Chu C W 1998 *Phys. Rev.* B **57** 2872
[24] Kimura T, Lawes G, Goto T, Tokura Y and Ramirez A P 2005 *Phys. Rev.* B **71** 224425
[25] Palkar V R, John J and Pinto R 2002 *Appl. Phys. Lett.* **80** 1628
[26] Mazumder R, Ghosh S, Mondal P, Bhattacharya D, Dasgupta S, Das N, Sen A, Tyagi A K, Sivakumar M, Takami T and Ikuta H 2006 *J. Appl. Phys.* at press
[27] Yang C-H, Koo J, Song C, Koo T Y, Lee K B and Jeong Y H 2006 *Phys. Rev.* B **73** 224112
[28] Ikeda N, Ohsumi H, Ohwada K, Ishii K, Inami T, Kakurai K, Murakami Y, Yoshii K, Mori S, Horibe Y and Kito H 2005 *Nature* **436** 1136